NUCLEAR THEORY, Vol. 40 (2023)
eds. M. Gaidarov, N. Minkov, Heron Press, Sofia

Shape Evolution in Palladium Isotopic Chain

Y. El Bassem[1,2], **M. El Adri**[1], **A. El Batoul**[1], **M. Oulne**[1]

[1]High Energy Physics and Astrophysics Laboratory, Department of Physics, Faculty of Sciences Semlalia, Cadi Ayyad University, P.O.B 2390, Marrakesh, Morocco

[2]ERMAM, Polydisciplinary Faculty of Ouarzazate, Ibn Zhor University, P.O.B 638, Ouarzazate, Morocco

Abstract. In this study, we explore the phenomenon of shape evolution in even-even $^{96-130}$Pd isotopes, employing the covariant density functional theory with two different parameterizations: the density-dependent meson-exchange DD-ME2 and the density-dependent point-coupling DD-PC1. This investigation is done on the basis of the evolution of the ground state shapes obtained within the axial and triaxial potential energy surface calculations. The shape transition in the palladium isotopic chain is conspicuously evident and distinct. Furthermore, various ground-state properties, including binding energy, two-neutron separation energy (S_{2n}), charge radii, and two-neutron shell gap (δ_{2n}), have been carefully calculated and found to be in good agreement with the available experimental data. Also, a strong shell closure is clearly seen at the magic neutron number $N = 82$.

1 Introduction

Currently, one of the primary focal points in both theoretical and experimental nuclear structure studies is the investigation of shape phase transitions in the ground state of atomic nuclei along isotopic chains. Neutron-rich nuclei within the mass range $A = 90 - 130$ on the nuclear chart have attracted particular attention from researchers. This region discloses a large number of interesting discoveries of new phenomena, such as proton radioactivity [1], cluster radioactivity [2], exotic shapes [3], island of inversion [4], giant halo near neutron dripline region [5], etc.

This specific mass region has garnered substantial interest and has been the subject of extensive theoretical and experimental investigations. From the theoretical side, both relativistic [6] and nonrelativistic [7, 8] approaches agree in the general description of the nuclear structural evolution in this mass region. It has been shown that the equilibrium nuclear shapes suffer rapid changes as a function of the number of nucleons with competing spherical, axially symmetric prolate and oblate, and triaxial shapes at close energies. This is supported experimentally by laser spectroscopy measurements [9] and spectroscopic studies [10, 11] as well as by 2^+ lifetime measurements [12, 13].

The evolution of nuclear structure has been extensively investigated through numerous theoretical studies employing different formalisms, this includes the relativistic mean-field (RMF) model [14,15], the interacting boson model (IBM) [16], and the self-consistent mean-field models with the Skyrme and the Gogny force [17–21].

Covariant density functional theory (CDFT) is one of the most attractive nuclear density functional theories based on energy density functionals. This theory has proven to be highly successful in accurately describing the ground- and excited-state properties of nuclei, encompassing both spherical and deformed configurations across the entire nuclear chart.

In this study, we have examined the shape evolution of even-even palladium (Pd, Z=46) isotopic chain across a broad spectrum of neutron numbers, ranging from N=50 up to N=84. The calculations were performed using the covariant density functional theory, employing two state-of-the-art functionals, namely the density-dependent point-coupling DD-PC1 [22, 23] and the density-dependent meson-exchange DD-ME2 [22, 24], which offer a comprehensive and precise depiction of various ground states and excited states across the entire nuclear chart [25–29].

The organization of this paper is as follows : In Section 2, a general overview of the theoretical formalism is presented. The numerical results of the calculations are discussed and compared in Section 3. Section 4 contains a brief summary of the principal results.

2 Theoretical Framework

The primary focus of this study is the microscopic description of the axial and triaxial shapes observed in neutron-rich Pd isotopes. The investigation has been carried out using two classes of covariant density functional models, namely the density-dependent meson-exchange (DD-ME) model, and the density-dependent point-coupling (DD-PC) model. The main differences between these two models revolve around the manner in which they handle the interaction range. DD-ME and DD-PC are both density-dependent models but the first has a finite interaction range, while the second uses a zero-range interaction with one additional gradient term in the scalar-isoscalar channel.

Within the meson-exchange model framework, the nucleus is treated as a system of Dirac nucleons that interact through the exchange of mesons with finite masses, resulting in finite-range interactions [30,31]. The isoscalar-scalar σ meson, the isoscalar-vector ω meson, and the isovector-vector ρ meson build the minimal set of meson fields for a quantitative description of nuclei. The meson-exchange model is defined by the standard Lagrangian density with medium dependence vertices [32]:

$$\mathcal{L} = \bar{\psi}\left[\gamma(i\partial - g_\omega\omega - g_\rho\vec{\rho}\vec{\tau} - eA) - m - g_\sigma\sigma\right]\psi + \frac{1}{2}(\partial\sigma)^2 - \frac{1}{2}m_\sigma^2\sigma^2 - \frac{1}{4}\Omega_{\mu\nu}\Omega^{\mu\nu} + \frac{1}{2}m_\omega^2\omega^2 - \frac{1}{4}\vec{R}_{\mu\nu}\vec{R}^{\mu\nu} + \frac{1}{2}m_\rho^2\vec{\rho}^2 - \frac{1}{4}F_{\mu\nu}F^{\mu\nu}, \quad (1)$$

where m is the bare nucleon mass and ψ denotes the Dirac spinors. m_σ, m_ω, and m_ρ are the masses of σ meson, ω meson, and ρ meson, respectively, with the corresponding coupling constants for the mesons to the nucleons as g_σ, g_ω, and g_ρ, respectively, and e is the charge of the proton and it vanishes for neutrons.

The point-coupling model represents an alternative formulation of the self-consistent Relativistic Mean Field (RMF) framework. [33–36]. The Lagrangian for the DD-PC model [24, 37] includes the free-nucleon Lagrangian, the point coupling interaction terms, and the coupling of the proton to the electromagnetic field and can be written as :

$$\begin{aligned}\mathcal{L} = \bar{\psi}\left(i\gamma\cdot\partial - m\right)\psi - \frac{1}{2}\alpha_S(\hat{\rho})\left(\bar{\psi}\psi\right)\left(\bar{\psi}\psi\right) \\ - \frac{1}{2}\alpha_V(\hat{\rho})\left(\bar{\psi}\gamma^\mu\psi\right)\left(\bar{\psi}\gamma_\mu\psi\right) - \frac{1}{2}\alpha_{TV}(\hat{\rho})\left(\bar{\psi}\vec{\tau}\gamma^\mu\psi\right)\left(\bar{\psi}\vec{\tau}\gamma_\mu\psi\right) \\ - \frac{1}{2}\delta_S\left(\partial_v\bar{\psi}\psi\right)\left(\partial^v\bar{\psi}\psi\right) - e\bar{\psi}\gamma\cdot A\frac{(1-\tau_3)}{2}\psi\,. \quad (2)\end{aligned}$$

The derivative terms in Eq. (2) account for the leading effects of finite-range interaction which are important in nuclei. In analogy with DD-ME model, this model contains isoscalar-scalar, isoscalar-vector and isovector-vector interactions (see Refs. [22, 24] for more details).

3 Results and Discussion

In this section, we provide a detailed microscopic description of the Pd isotopic chain, spanning from neutron number $N = 50$ to $N = 84$. Our analysis involves performing constrained calculations to obtain the axial and triaxial potential energy surfaces (PESs), along with studying various ground-state properties. To carry out these calculations, we utilized the density-dependent effective interactions DD-ME2 and DD-PC1.

In Figure 1, we display for each even-even Pd isotope (covering the mass interval $96 \leqslant A \leqslant 130$) the potential energy curves (PECs) as a function of the deformation parameter, β_2, obtained within the CDFT framework by using DD-ME2 and DD-PC1 interactions. Positive values of β_2 correspond to a prolate deformation and negative values to an oblate deformation.

As we can see from Figure 1, the isotope ^{96}Pd, which corresponds to the shell closure at the neutron magic number $N = 50$, has a spherical shape. The next isotope, ^{98}Pd, starts to develop two shallow degenerate minima, prolate and oblate, that correspond to a small value of β_2. The $^{100-108}$Pd isotopes show a similar structure, with a well-deformed prolate minimum, $\beta_2 \approx 0.2$, and an oblate local minimum.

A transition from prolate to oblate shapes occurs smoothly between ^{108}Pd(prolate) and ^{110}Pd(oblate). In $^{112-118}$Pd two minima appear, with a well-deformed oblate minimum, $\beta_2 \approx -0.25$, and a prolate local minimum. As the mass number increases, the two well-deformed minima gradually disappear and we get a

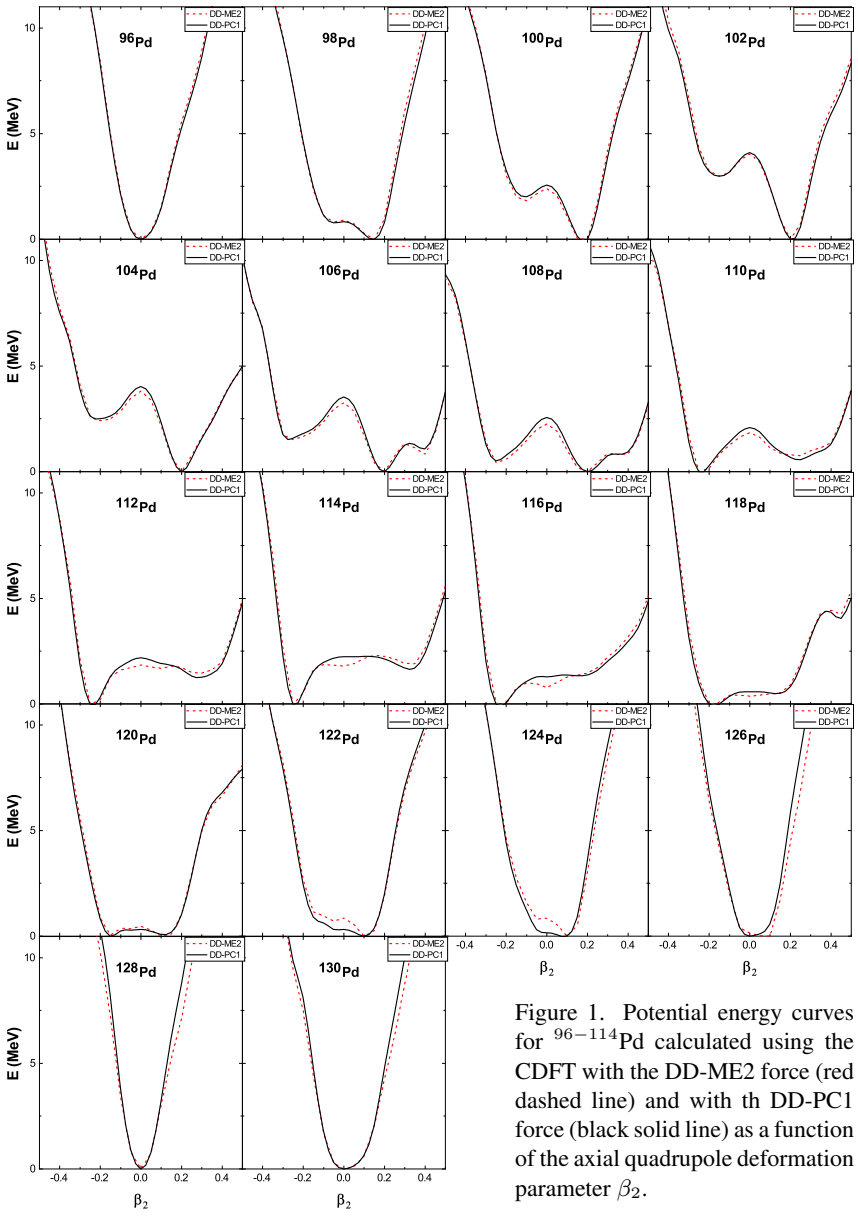

Figure 1. Potential energy curves for $^{96-114}$Pd calculated using the CDFT with the DD-ME2 force (red dashed line) and with th DD-PC1 force (black solid line) as a function of the axial quadrupole deformation parameter β_2.

sharp single minimum at ^{128}Pd, which confirms the spherical shape at the magic neutron number $N = 82$.

To investigate the dependence on γ, potential energy surfaces (PESs) have been computed for Pd isotopes across the neutron number range from $N = 50$ to $N = 84$ in the $(\beta_2; \gamma)$ plane, where β_2 quantify the deformation of the nucleus

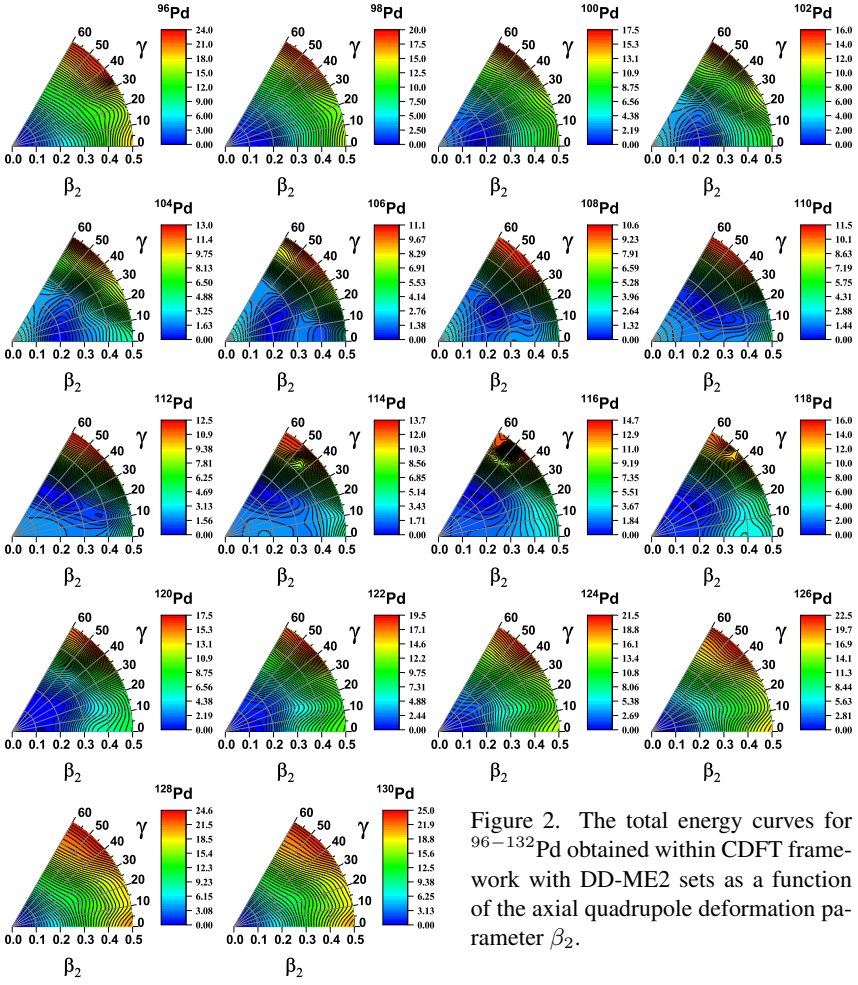

Figure 2. The total energy curves for $^{96-132}$Pd obtained within CDFT framework with DD-ME2 sets as a function of the axial quadrupole deformation parameter β_2.

while γ measures the degree of triaxiality. The systematic process involves performing constrained triaxial calculations that map the quadrupole deformation space defined by β_2 and γ, employing DD-ME2 and DD-PC1 effective interactions.

In Figure 2 and Figure 3 we display the triaxial contour plots of $^{96-130}$Pd isotopes in the $\beta_2 - \gamma$ plane using DD-ME2 and DD-PC1 parametrizations, respectively. Energies are normalized with respect to the binding energy of the global minimum.

From Figures 2 and 3, one can notice that the shape transition is very evident. It starts from the spherical (^{96}Pd) to prolate ($^{98-104}$Pd) deformation, and to triaxial ($^{106-112}$Pd) deformation, then shifted to oblate (^{114}Pd) deformation. The isotopes ($^{116-120}$Pd) are characterized by a certain degree of triaxiality.

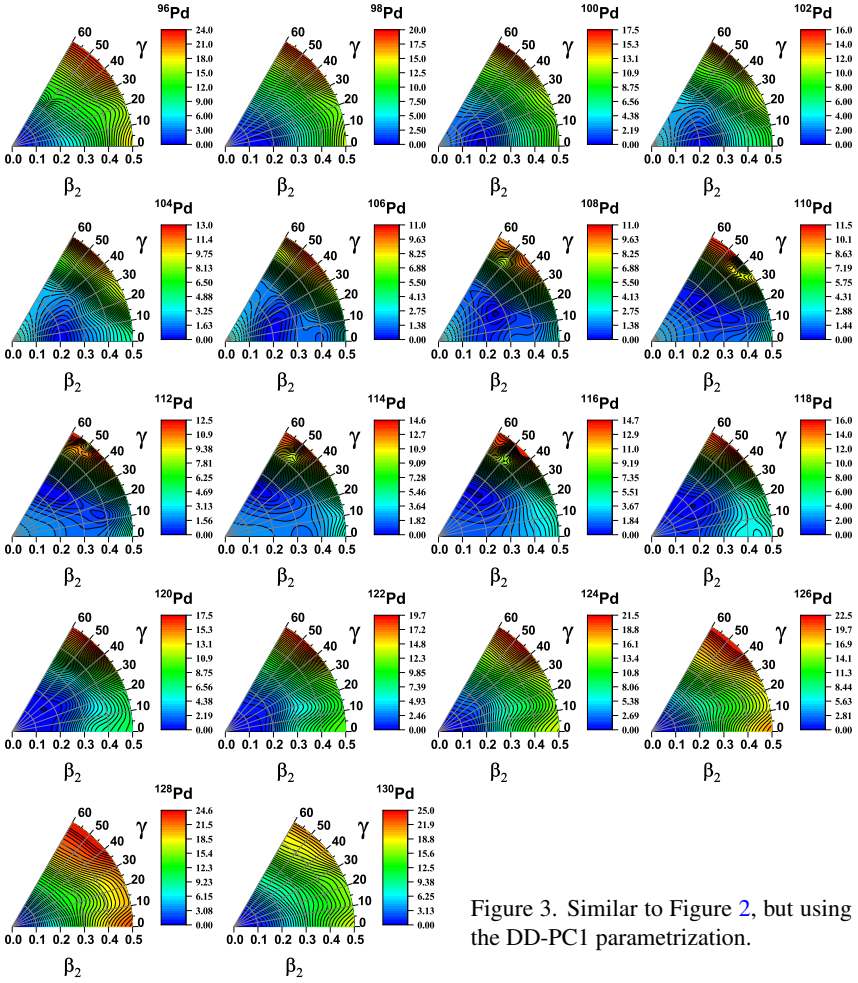

Figure 3. Similar to Figure 2, but using the DD-PC1 parametrization.

Afterwards, it evolves towards a prolate deformation ($^{122-124}$Pd), and finally the spherical shape is regained at ($^{126-130}$Pd) in the vicinity of the shell closure at the neutron magic number $N = 82$. These results are in good agreement with the results shown in Figure 3 of Ref. [38]

The shape evolution observed in Pd isotopes in this section can be attributed to changes in the values of several physical properties of the ground state, including binding energy (BE), two neutron separation energies (S_{2n}), charge radii (R_c) and two-neutron shell gap δ_{2n}. In Figures 4, 5, 6 and 7 we present these physical properties as a function of the neutron number N in comparison with the available experimental data.

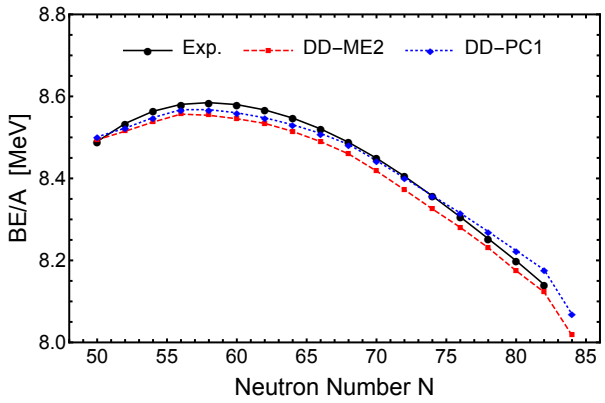

Figure 4. The binding energies per nucleon for even-even $^{96-130}$Pd isotopes.

The binding energy per nucleon (BE/A) of ground states for palladium isotopes, $^{96-130}$Pd, are presented in Figure 4 as a function of the neutron number N. The available experimental data [39] are also shown for comparison.

From Figure 4 it can be clearly seen that the experimental data are accurately reproduced by the theoretical predictions.

The two-neutron septation energy, $S_{2n}(N,Z)$ = BE(N,Z) - BE$(N-2,Z)$, is plotted in Figure 5 as a function of the neutron number (N). The available experimental data [39] are also shown for comparison.

As one can see from Figure 5, the results of the two density-dependent models DD-ME2 and DD-PC1 reproduce the experimental data very well. S_{2n} grad-

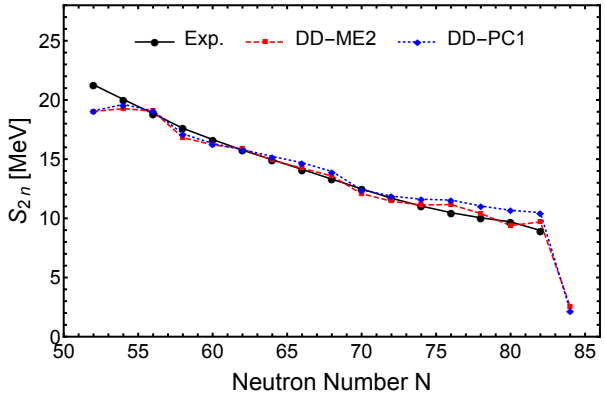

Figure 5. The two-neutron separation energies S_{2n}, for even-even $^{96-130}$Pd isotopes, obtained with DD-ME2 and DD-PC1, and compared with the available experimental data [39].

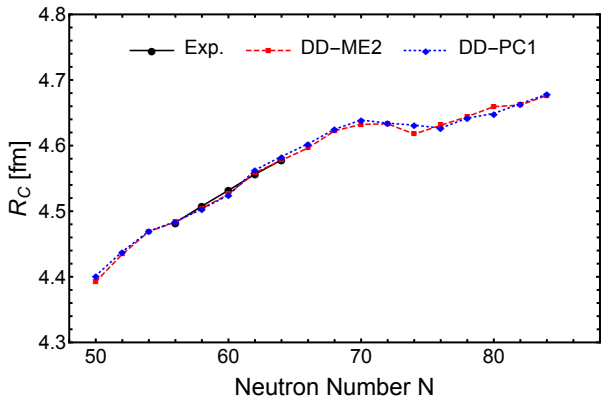

Figure 6. The charge radii of Pd isotopes.

ually decreases with N, and a sharp drop is clearly seen at $N = 82$, which indicates the closed shell at this magic neutron number.

Figure 6 shows the charge radii calculated within CDFT with DD-ME2 and DD-PC1 in comparison with the available experimental data [40]. The theory and experiment exhibit a strong and evident agreement.

The two-neutron shell gap $\delta_{2n} = S_{2n}(N, Z) - S_{2n}(N + 2, Z)$ is a more sensitive observable for locating the shell closure. The variation of δ_{2n} as a function of the neutron number N is shown in Figure 7. The sharp peak in (δ_{2n}) clearly seen at $N = 82$ indicates the shell closure at this neutron magic number.

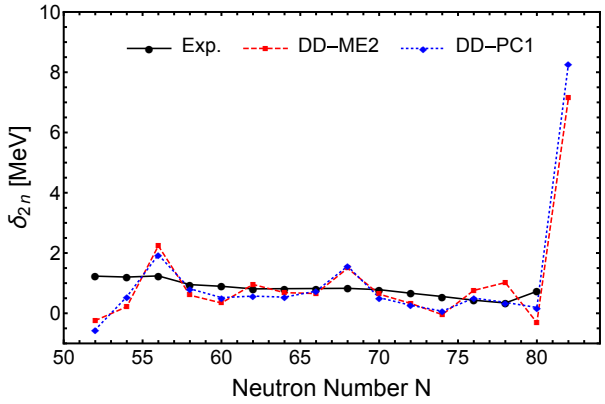

Figure 7. The two-neutron shell gap δ_{2n} for even-even $^{96-130}$Pd isotopes.

4 Conclusion

In this work, we have investigated the structural evolution with the increase of the number of neutrons in the isotopic chain of palladium, $^{96-130}$Pd, within the framework of the CDFT, by using DD-PC1 and DD-ME2 functionals.

The analysis of the shape transition is done on the basis of the evolution of the ground state shapes obtained within axial and triaxial potential energy surface calculations. The transition from a spherical to a deformed shape is prominently evident in the isotopic chain.

Some ground state properties such as binding energy, two-neutron separation energy (S_{2n}), charge radii and two-neutron shell gap (δ_{2n}) have been calculated and have been found to be in good agreement with the experimental data. The observed smooth change in the ground state deformation is correlated with a gradual evolution of the physical properties in the ground state. A distinct and robust shell closure is evident at $N = 82$.

Acknowledgment

This research was supported through computational resources of HPC-MARWAN (hpc.marwan.ma) provided by the National Center for Scientific and Technical Research (CNRST), Rabat, Morocco.

References

[1] B. Blank, M. Borge, *Prog. Part. Nucl. Phys*. **60** (2008) 403.
[2] Raj K. Gupta, W. Greiner, *Int. J. Mod. Phys.* **03** (1994) 335.
[3] L.P. Gaffney *et al.*, *Nature (London)* **497** (2013) 199.
[4] O.B. Tarasov *et al.*, *Phys. Rev. Lett*. **102** (2009) 142501.
[5] J. Meng, P. Ring, *Phys. Rev. Lett.* **80** (1998) 460.
[6] H. Mei, J. Xiang, J.M. Yao, Z.P. Li, J. Meng, *Phys. Rev. C* **85** (2012) 034321.
[7] M. Bender, K. Bennaceur, T. Duguet, P.-H. Heenen. T. Lesinski, J. Meyer, *Phys. Rev. C* **80** (2009) 064302.
[8] A. Ait Ben Mennana, Y. EL Bassem, M. Oulne, *Phys. Scr.* **95** (2020) 065301.
[9] B. Cheal, K.T. Flanagan, *J. Phys. G: Nucl. Part. Phys.* **37** (2010) 113101.
[10] C.Y. Wu *et al.*, *Phys. Rev. C* **70** (2004) 064312.
[11] T. Sumikama *et al.*, *Phys. Rev. Lett.* **106** (2011) 202501.
[12] H. Mach *et al.*, *Phys. Lett. B* **230** (1989) 21.
[13] C. Goodin *et al.*, *Nucl. Phys. A* **787** (2007) 231c.
[14] M. Bhuyan, *Phys. Rev. C* **92** (2015) 034323.
[15] H. Abusara, Shakeb Ahmad, *Phys. Rev. C* **96** (2017) 064303.
[16] K. Nomura, R. Rodriguez-Guzman, L.M. Robledo, *Phys. Rev. C* **94** (2016) 044314.
[17] M. Bender, G.F. Bertsch, P.-H. Heenen, *Phys. Rev. C* **73** (2006) 034322.
[18] Y. El Bassem, M. Oulne, *Int. J. Mod. Phys. E* **24** (2015) 1550073.
[19] Y. El Bassem, M. Oulne, *Nucl. Phys. A* **957** (2017) 22.
[20] Y. El Bassem, M. Oulne, *Int. J. Mod. Phys. E* **26** (2017) 1750084.

[21] M. El Adri, M. Oulne, *Eur. Phys. J. Plus* **135** (2020) 1-16.
[22] T. Nikšić, N. Paar, D. Vretenar, P. Ring, *Comput. Phys. Commun*. **185** (2014) 1808.
[23] G.A. Lalazissis, T. Nikšić, D. Vretenar, P. Ring, *Phys. Rev. C* **71** (2005) 024312.
[24] T. Nikšić, D. Vretenar, P. Ring, *Phys. Rev. C* **78** (2008) 034318.
[25] A. Karim, S. Ahmad, *Phys. Rev. C* **92** (2015) 064608.
[26] Y. El Bassem, M. Oulne, *Nucl. Phys. A* **987** (1999) 16.
[27] Y. El Bassem, M. Oulne, *Int. J. Mod. Phys. E* **28** (2019) 1950078.
[28] A. Ait Ben Mennana, R. Benjedi, R. Budaca, P. Buganu, Y. ELBassem, A. Lahbas, M. Oulne, *Phys. Scr.* **96** (2021) 125306.
[29] A. Ait Ben Mennana, R. Benjedi, R. Budaca, P. Buganu, Y. El Bassem, A. Lahbas, M. Oulne, *Phys. Rev. C* **105** (2022) 034347.
[30] S. Typel, H.H. Wolter, *Nucl. Phys. A* **656** (1999) 331.
[31] G. A. Lalazissis, S. Karatzikos, R. Fossion, D. Pena Arteaga, A.V. Afanasjev, P. Ring, *Phys. Lett. B* **671** (2009) 36.
[32] Y.K. Gambhir, P. Ring, A. Thimet, *Ann. Phys. (NY)* **198** (1990) 132.
[33] P. Manakos, T. Mannel, *Z. Phys. A-Atomic Nuclei* **330** (1988) 223.
[34] J.J. Rusnak, R.J. Furnstahl, *Nucl. Phys. A* **627** (1997) 495.
[35] T. Bürvenich, D.G. Madland, J.A. Maruhn, P.G. Reinhard, *Phys. Rev. C* **65** (2002) 044308.
[36] P.W. Zhao, Z.P. Li, J.M. Yao, J. Meng, *Phys. Rev. C* **82** (2010) 054319.
[37] B.A. Nikolaus, T. Hoch, D.G. Madland, *Phys. Rev. C* **46** (1992) 1757.
[38] T. Naz, G.H. Bhat, S. Jehangir, S. Ahmad, J.A. Sheikh, *Nucl. Phys. A* **979** (2018) 1.
[39] M. Wang, G. Audi, A.H. Wapstra, F.G. Kondev, M. MacCormick, X. Xu, B. Pfeiffer, *Chin. Phys. C* **36** (2012) 1603 .
[40] I. Angeli, *At. Data Nucl. Data Tables* **87** (2004) 185-206.